RESEARCH PAPER

# Survey and Investigation of Nanostructure Hardystonite/Biphasic Calcium Phosphate to Use in Biomedical Engineering

***Hassan Gheisari Dehsheikh[1,2*] and Ebrahim Karamian[1]***

*[1] Advanced Materials Research Center, Department of Materials, Najafabad Branch, Islamic Azad University, Najafabad, Iran*

*[2] Faculty of Science Research, University of Toronto, Toronto, ON, Canada, M5S3G3*

**ARTICLE INFO**

***Article History:***
*Received 17 October 2019*
*Accepted 21 January 2020*
*Published 15 February 2020*

***Keywords:***
*Nanostructure*
*Hardystonite*
*Calcium phosphate*
*In vitro*
*TEM*
*SEM*

**ABSTRACT**

The development of structures serving as scaffolds to fill bone defects, and promote bone regeneration is of a particular importance in bone tissue engineering. In this study, highly porous (≈75%) nanostructured hardystonite/biphasic calcium phosphate scaffolds (BCPS) with interconnected porosity were developed using various hardystonite contents via the space holder technique. Transmission electron microscopy (TEM), X-ray diffraction (XRD) and scanning electron microscopy (SEM) techniques were employed to evaluate different samples. In addition, the role of scaffold composition on the mechanical performance, bioactivity and biodegradability was studied. The results showed that the scaffolds produced have an average pore size of 350 nm and a density between 2.2 ± 0.4 and 1.7 ± 0.2 gr/cm$^3$, depending on the hardystonite contents. Furthermore, increasing the hardystonite content of scaffolds from 0 (control) to 30 wt. % enhanced the bioactivity test, biodegradability, and compressive strength from 1.1 ± 0.1 to 3.1 ± 0.2 MPa, respectively. Our project suggests that nanostructured hardystonite/BCPS with improved biological and mechanical properties could potentially be used for biomedical engineering such as bone tissue engineering application.

**How to cite this article**
*Gheisari Dehsheikh H. Survey and Investigation of Nanostructure Hardystonite/Biphasic Calcium Phosphate to Use in Biomedical Engineering. Nanochem Res, 2020; 5(1):35-45. DOI: 10.22036/ncr.2020.01.004*

## INTRODUCTION

Scaffolds with desired biocompatibility, biodegradability and mechanical behavior have been of a great interest to many scientists [1]. The mechanical properties mismatch between bone and scaffolds can inversely affect the implant function in vivo. Bone tissue engineering is seeking to regenerate bone defects through combining cells, biocompatible scaffolds and growth factors [2]. Scaffolds with poor mechanical properties may fail under load bearing applications, while scaffolds with higher mechanical behavior to that of bone may cause stress shielding, bone resorption and poor osseointegration [3]. Another crucial parameter that should be considered in the synthetic bone scaffolds is porosity. Pore size in the range of 150-600 μm is necessary for neovascularization, and cell-migration [4]. Natural hydroxyapatite with chemical formula Ca10 $(PO_4)_6(OH)_2$ is one of the best candidates to develop bone scaffolds for tissue engineering due to its unique properties such as good biocompatibility and chemical composition similar to that of bone [5]. However, because of the low degradation rate and poor mechanical properties, various research has been conducted on the development of new bioceramics such as tri-calcium-phosphate (TCP),titania and silicon-carbide with improved mechanical strength and biodegradability compared to pure hydroxyapatite (HA) [6,7]. Recently, Beta-tri-calcium-phosphate

* Corresponding Author Email: *hassan.gh.d@gmail.com*

(ß-TCP) has shown a great biocompatibility and biodegradability which resorbs faster than hydroxyapatite (HA) in the defect location promoting the healing process [2,8]. However, due to high bioactivity, osteoconductivity, and controllable degradation rate, BCP ceramics have been more favorable than pure HA and b-TCP alone to repair periodontal defects or as bone graft replacements [3, 4, 9]. As regards, similar to other calcium phosphate ceramics (CPS), their strength is not acceptable for load bearing applications [5].

Recently, silicon-magnesium based bio-ceramics have drawn interests in the development of bone implant materials [6,7,8]. While zinc (Zn) is an essential element of bone, silicon (Si) is involved in human bone metabolism [10]. Hardystonite (HT) with the chemical formula of $Ca_2ZnSi_2O_7$ is a silicate-based bio-ceramic utilized for artificial bone and dental root as a result of its great hydroxyapatite formation ability and higher mechanical properties compared to HA [11,12]. Furthermore, it has been reported that glassceramics consisting of eutectic phase, with the composition of 40 wt% TCP and 65 wt. % hardystonite [13, 14].

Biphasic calcium phosphate scaffolds (BCPS) have been successfully fabricated utilized camphene-based freeze-casting and a combination of gel-casting and polymer sponge techniques. Space holder approach has been widely used to develop metallic scaffolds. In this method, spacer particles such as carbamide (CO (NH2)2), ammonium hydrogen carbonate (NH4HCO3) and sodium chloride (NaCl) are mixed with the main powder to form porosity during the sintering process. Also, limited ceramic based scaffolds have been fabricated using this method.

The aim of the present study is to produce nanostructured hardystonite/biphasic calcium phosphate scaffolds (HT)/(BCPS) by the space holder technique. Also, the influence of Hardystonite with different contents on the average pore size, porosity, microstructures and mechanical behavior of the scaffolds will be discussed. In addition, the effects of (HT) nanopowder on the in situ formation of BCPS will be evaluated.

## MATERIALS AND METHODS

*Formation of hydroxyapatite (HA) and hardystonite (HT) nanopowders*

Hardystonite (HT) was synthesized via the sol-gel technique based on the previous study . In short, calcium nitrate tetra-hedrate from Merk Co. and magnesium nitrate hexahydrate from Merk Co. with similar molarity (0.127M) were dissolved into 250 cc ethanol and sintered at 90 ˚C for 45 minutes. Tetraethyl orthosilicate (TEOS) (0.25 M) from Merk co was added to the above homogeneous solution and slowly stirred to obtain a gel network. The gel was dried at 110 ˚C for 36 h and then calcined at 900 ˚C for 3 hours. The powder was ball milled for 3 h in a planetary ball-mill machine from Santam Sanat Co, in zirconia cup. Also, hydroxyapatite (HA) nano-powder was synthesized using sol gel technique, according to previous study. Appropriate amounts of Ca (NO) $S_4H_2O$ and phosphoric pentoxide (from Merck Co) was separately dissolved in absolute ethanol to form 1.76 and 0.6 mol/l solutions, respectively. The two solutions were mixed and stirred at room temperature for 36 h and then the obtained clear gel was dried at 90 ˚C in an electrical oven for about 36 h. Dried gel was calcined at 800 ˚C for 30 min in a muffle furnace by a heating rate of 6 ˚C /min. Hydroxyapatite (HA) nanopowder was partially decomposed to tri-calcium phosphate (TCP) during sintering at high temperature.

*Synthesis of nanostructure Hardystonite/biphasic calcium phosphate scaffolds (HT/BCPS)*

Hardystonite/BCPS was produced using space holder technique. In first part, as synthesized hydroxyapatite and hardystonite nanopowders were blended with various weight ratios (100:0 , 90:10 , 80:20 and 70:30) in a high energy ball-milling (HEBM) for 2 h in a zirconia jar.

Also, in order to develop composite scaffolds (CS), sodium chloride (NaCl from Sigma Co) was used as a spacer agent. Sodium choloride and composite powders with a weight ratio of 70:30 was mixed together. The prepared powder was uniaxially pressed into pellets in a hardened steel mould at a pressure of 300 MPa for 2 min using 6 wt% polyvinyl alcohol solutions as a binder. The green bulks were annealed at 1200 ˚C for 3 h with the heating and cooling rate of 3 ˚C /min in order to remove the NaCl particles. The samples were sintered at 1250 ˚C for 3 h with heating and cooling rate of 5 ˚C /min. Table 1 shows the designation and specification of samples.

*Investigation of nanopowders and scaffolds*
*Physical characterization*

In this part, phase transformation and crystallite size of the synthesized powders and scaffolds were

Table 1. Determination and characteristics of various scaffolds

| Designation | Hardystonit Contents (wt%) | -TCP (wt%)ß | Apparent Porosity (AP%) | Real Density (RD %)(g/cm$^3$) | Apparent Density (AD)(%) |
|---|---|---|---|---|---|
| BCPS 0 (Control) | 0 | 31 | 81 (±3) | 3.14 | 1.7 (±0.4) |
| BCPS 10 | 10 | 24 | 81 (±1.4) | 3.16 | 2.187 (±0.9) |
| BCPS 20 | 20 | 18 | 78 (±1.6) | 3.18 | 2.5 (±0.14) |
| BCPS 30 | 30 | 14 | 75 (±4) | 3.18 | 2.41 (±0.29) |

estimated using a Hitachi 2300-SWE00, XRD with Cuka radiation (40 kV, 30 mA, step size of 0.05, scan rate of 1/min, 20<2Θ < 80) from Germany. The average crystallite size was estimated in the synthesized powders and scaffolds using modified Scherrer equation as follow:

$$ß = \frac{k.ħ}{t.\cos\Theta} \quad (1)$$

Where ß is the full-width at half maximum intensity, ħ is the wavelength (ħ = 0.154056 nm), Θ is the Bragg's angle (˚), K is a constant (K = 0.89), and t is the apparent crystallite size (nm). For this purposes, three diffraction peaks of (212), (012), and (400) were

selected. The half width of peaks was calculated using sigma plot software. The crystallinity of hydroxyapatite (HA) powder was also estimated from the x-ray diffraction data using Eq. (2) [28]:

$$X_C = 1 - (\frac{V112/300}{I300}) \quad (2)$$

Where Xc is the degree of HA crystallinity, I300 is the intensity of the (300) diffraction peaks, and V112/300 is the intensity of the shoulder between the (112) and (300) diffraction peaks. Additionally, the ß-TCP value was quantitatively evaluated using x-ray diffraction patterns as follows:

$$X_i = \frac{Iei.\mu j}{Kei} \quad (3)$$

where $X_i$ is the weight fraction of phase, i in sample $I_{ei}$ is the intensity of xrd peak of the phase i in the xrd pattern, $\mu_i$ is the average mass absorption coefficient of the sample , and $K_{ei}$ is a constant which depends on the nature of the phase.

The transmission electron microscopy (TEM, Zaies, Switzerland, 2080, 200KV) was also used to determine the morphology and particle size of the synthesized hydroxyapatite (HA) and Hardystonite (HT) powders. Furthermore, the average particle size of the nanopowders was estimated via images obtained. The morphology of the powders as well as the fracture surface of the samples and energy dispersive spectrometry (EDS-EDX) elemental maps were investigated using scanning electron microscope (SEM, Hitach, Japan KV45). Also, to create a conductive layer of metal on the samples and prevent charging of the specimens and reduce thermal damages, the samples were sputter-coated with a thin layer of gold metal. The apparent density (AP) and true density as well as the apparent porosity (AP) of the scaffolds were estimated using Archimedes formula based on the following equations:

$$\text{Apparent Porosity (AP)} = \frac{Ww-Wd}{Ww-Ws}\times 100 \quad (4)$$

$$\text{Apparent Density (AD)} = \frac{Wd}{Ww-Ws}\times 100$$

Where $w_w$ is the wet weight, $w_d$ is the dry weight and $w_s$ is the wet weight suspended in water.

$$\text{Real Density (RD)} = \frac{WHA}{WHA+WHT}\times \rho_{HA} + (\frac{WHT}{WHA+WHT} \times \rho_{HT}) \quad (5)$$

where $W_{HA}$ is the weight of hydroxyapatite (HA), $W_{HT}$ is the weight of hardystonite (HT) and ρ is density. All experiments were carried out in triplicates.

*Mechanical characterization*

To measure the strength of the samples with the height and diameter of 30 mm were produced and then subjected to a compression test using a universal testing machine (Sanam sanat Co, K40XV) at a crosshead speed of 0.6 mm/min.

*Evaluation of In vitro bioactivity and biodegradability*

In order to evaluate the In vitro bioactivity and biodegradability, a simulated body fluid (SBF) containing ion concentration similar to those available in human blood plasma was prepared according to a procedure described previously. The

scaffold samples were soaking in simulated body fluid at 37˚C for 1, 3, 7, 14, 21 and 28 days. During the soaking time, the changes in the pH value of the solutions were calculated via a pH meter (Hitachi, Japan). In addition, the concentration of calcium and phosphorus ions in simulated body fluid was evaluated after soaking the scaffolds for 28 days using inductive coupled plasma (ICP, Zaies, Switzerland). After soaking, the scaffolds were dried at 60 ˚C for 1 day. SEM and EDS were used to study the hydroxyapatite formation ability and morphology of precipitates on the surface of the scaffold samples. Degradation rate of scaffolds were also investigated in buffered saline solution at pH ¼ 7.4 ± 0.03 and temperature of 36 ± 0.8 ˚C for 28 days. Buffer solution was changed every 3 days. In specific time intervals (7, 14, 21, and 28 days), the scaffolds were removed from the buffer solution, and dried in an electrical oven at 80 ˚C for 24 h. The weight loss (wl %.) of the samples was calculated as follows :

$$\text{Weight loss (\%)} = \frac{(wi - wf)}{wi} \times 100 \quad (6)$$

Where $w_i$ is the weight of the scaffold samples before soaking and $w_f$ is the weight of dry sample after being soaked.

## RESULTS AND DISCUSSION

The results of studies on hydroxyapatite (HA) and hardystonite (HT) nanopowders are shown in Fig. 1; the X-ray diffraction patterns, scanning

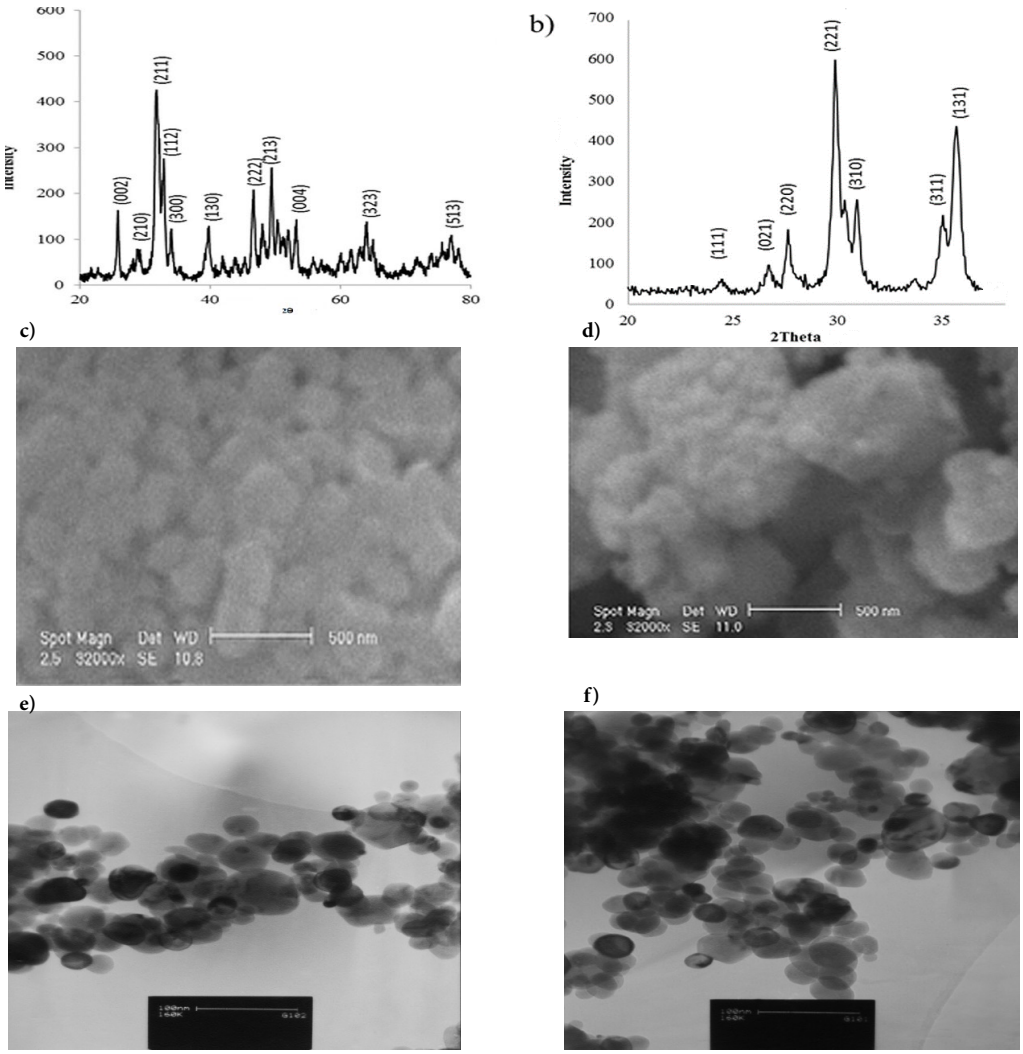


Fig. 1 X-Ray diffraction patterns (a , b), SEM images (c , d) and TEM micrographs (e , f) of HA (a, c, and e) and HT (b, d and f) nanopowders synthesized by the sol gel method.

electron microscopy images and transmission electron microscopy of hydroxyapatite (HA) and hardystonite (HT) nanopowders synthesized using sol gel method. Based on the XRD patterns, pure hydroxyapatite (XRD JCPDS data file No, 00-019-0239) (Fig. 1a) and hardystonite (HT) (XRD JCPDS data file No. 01-003-0865) (Fig. 1b) nanopowders were synthesized without any secondary phases. In addition, the average crystallite sizes of the (HA) and (HT) nanopowders obtained via modified Scherer equation were about 19.8 nm and 31.0 nm, respectively. Also, the crystallinity of HA powder calculated from the XRD pattern using Eq. (5) was about 75%. As can be seen in Fig. 1c and d, HA and HT nanopowders showed a spherical morphology with the agglomerated particles smaller than 100 nm (about 21 nm). As can be seen in the transmission electron microscopy(TEM) (Figs. 1e and f), while the HA powder consisted of homogenous spherical particles with the average size of 18 ± 3 nm, the particles of HT powder was irregular in shape with the average size of 36 ± 2 nm.

*Survey of composite scaffolds (CS)*

The x-ray diffraction patterns of various scaffolds with different HT contents after sintering at 1250 ˚C for 3 h were recorded. According to the XRD patterns, the composite consists of HA and beta-tri calcium phosphate (ß-TCP) as the main phases and a small amount of HT phase enhanced with increasing the content of HT nanopowder. So, the presence of ß-TCP in the XRD patterns demonstrated the decomposition of HA during the sintering at high temperature. Furthermore, some ∝ -TCP peaks could be detected in all the XRD patterns, suggesting that further phase transformation of ß-TCP phase is a low temperature polymorph of TCP which could be transformed to ∝ -TCP at high temperatures. In addition, the ratio of hydroxyapatite to ß-TCP varied in different compositions demonstrating the effects of HT contents on the decomposition degree of hydroxyapatite ceramic. Also, Table 1 shows the amounts of ß-TCP for various composites. As can be seen, with increasing the HT content the amount of ß -TCP decreased, which is in a good agreement with the results obtained by other researchers who pointed out that incorporation of HT within HA matrix could suppress the decomposition of HA to TCP. Furthermore, HA/TCP ratio could be easily controlled via the addition of secondary agents such as HT in this research. So, based on the XRD patterns obtained from the scaffold samples (Fig. 2), the average crystallite sizes of HA in the

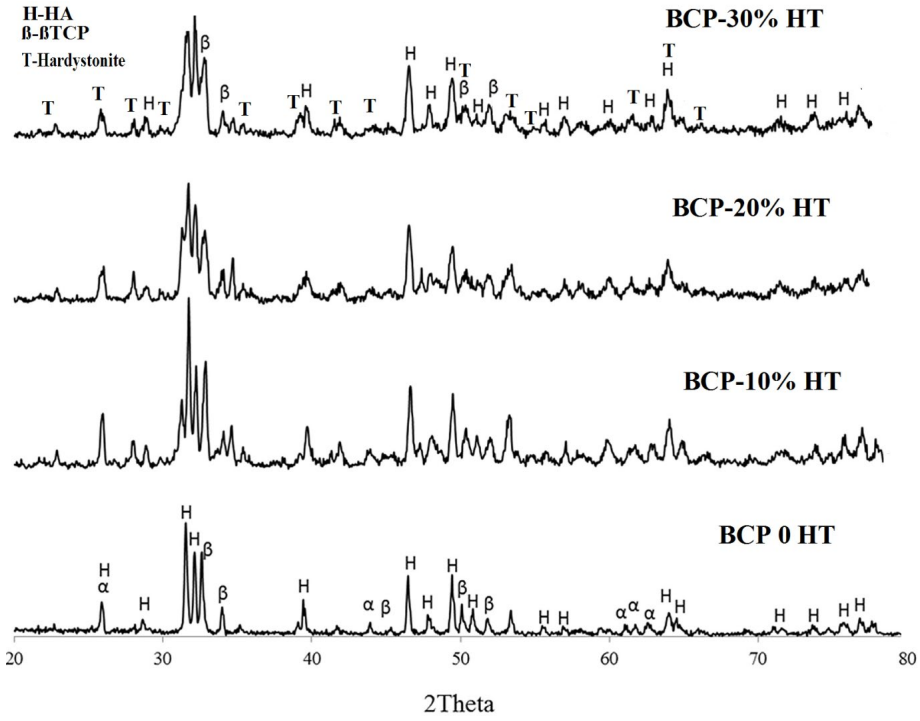


Fig. 2. The X-ray diffraction patterns of the scaffolds consisting of various hardystonite (HT) contents sintered at 1300 ˚C for 3 h.

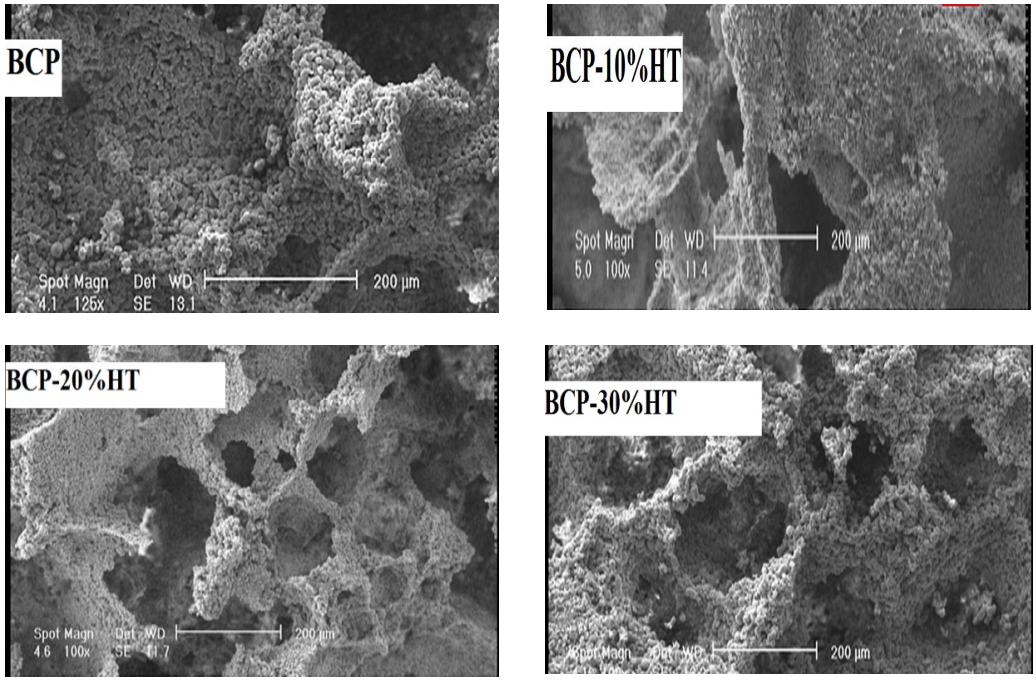


Fig. 3. Scanning electron microscopy images at 1300 ˚C for 3 h.

composite scaffolds were about 31.0 ± 3.5, 32.0 ± 1.1, 28.0 ± 2.8 and 24.0 ± 3.1 nm for BCP based scaffolds consisting of 0, 10, 20 and 30 wt% of hardystonite (HT) nanopowder, respectively (Eq. (1)). The scanning electron microscopy (SEM) images are shown in Fig. 3. Images with low magnification confirmed the formation of interconnected pores, which homogenously distributed throughout the samples. The average pores size of the scaffolds (Fig. 4a) reduced with increasing the HT content from 350 ± 80 µm to 200 ± 50 µm, which may boost bone ingrowth. Higher magnification images also demonstrated the formation of micropores throughout the scaffolds. The sintering temperature of the specimens was selected near the melting point of HT at 1300 ˚C. Thus, HT nanopowder can act as a sintering aid to improve the mechanical behavior of the scaffold samples. So, these results were in excellent agreement with other studies reported the role of HT in HT/HA bulk composites as a sintering agent. Also, the average grain size of the scaffolds in different composites also demonstrated the effects of HT on the suppression of grain growth (Fig. 4b). With increasing the HT content from 0 to 30 wt%, the average grain size of the scaffolds decreased from 7 ± 0.8 µm to 2 ± 0.5 µm, respectively. While

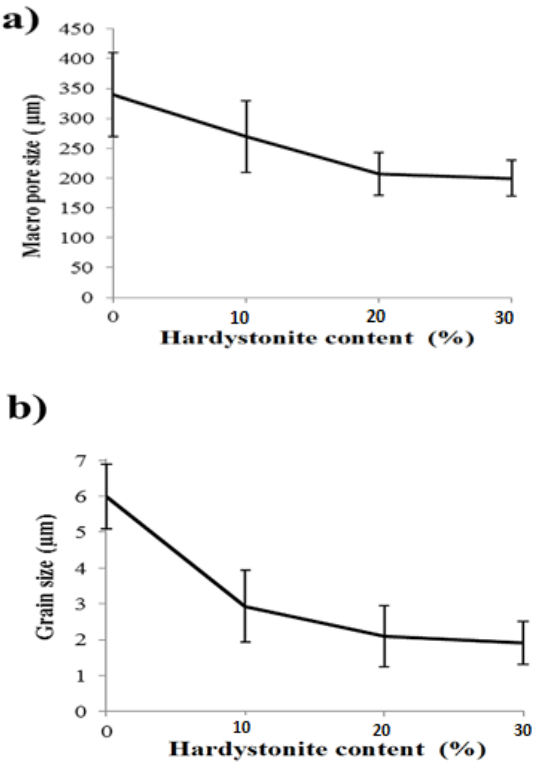


Fig. 4. Graphs of average a) macrospore and b) grain size of various composite scaffolds as a function of hardystonite (HT) contents.

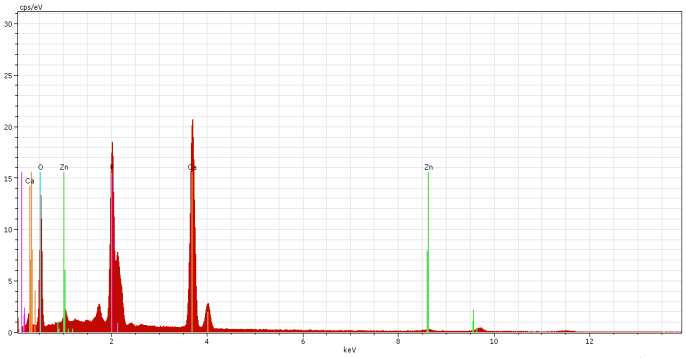


| Element | series | [wt.%] | orm. wt.%] | orm. at.%] |
|---|---|---|---|---|
| Oxygen | K-series | 43.08311 | 46.10041 | 67.0643 |
| Silicon | K-series | 0.770121 | 0.824056 | 0.682912 |
| Phosphorus | K-series | 10.61332 | 11.35661 | 8.533856 |
| Calcium | K-series | 36.87211 | 39.45442 | 22.91289 |
| Zinc | K-series | 2.116294 | 2.264507 | 0.806033 |
| | Sum: | 93.45495 | 100 | 100 |

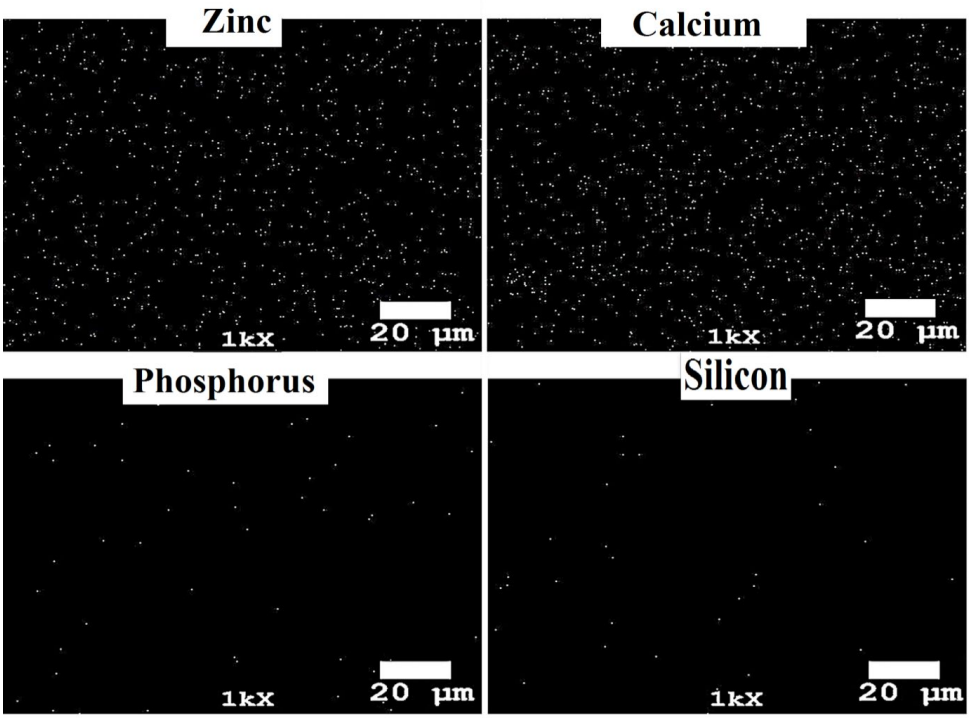


Fig. 5. Energy dispersive spectrometry mapping nanostructured BCPS 30 after sintering at 1300 ˚C for 3 h.

biphasic calcium phosphate grains started to necking, composite scaffolds were mostly densified, specifically at BCPS30 sample. The presence of HT in the BCPS matrix can simultaneously improve the sintering behavior and suppress the grain growth. Similar observations were reported in other studies regarding the presence of HT in alumina matrix which resulted in a decrease in the grain growth of alumina and an improvement in the densification rate. As seen, the average density and porosity of the scaffolds were calculated based on the Archimedes formula in (Table 1). The

density of the scaffolds was improved with increasing the HT content, confirming the role of HT agent in the reduction of micropores in the wall of scaffolds and improvement of scaffolds densification (Fig. 3). Also, Fig. 5 shows the energy dispersive spectrometry mapping of Ca, P, Zn and Si elements in the BCPS30 scaffold after sintering at 1300 ˚C for 3 h. As seen, HT nanopowder was well distributed in the BCP matrix. So, EDS micro-analysis demonstrated that NaCl particles were not remained in the scaffolds, hence, this technique can be a suitable for fabrication of ceramic based scaffolds. The Ca/P ratio obtained from the EDS analysis was about 1.42 which shows the decomposition of hydroxyapatite and the well distribution of HT phase in the constructs. So, based on Table 1 and Fig. 4, introducing HT nanopowder into the BCPS matrix could act as a sintering aid leading to a smaller micropore size, and denser struts while preventing from grain growth during the sintering process. Accordingly, based on the results, decomposition of HA to TCP could be prohibited by adding HT to the matrix, followed by improving the mechanical behavior of the scaffold samples. The success rate in bone replacement surgeries depends on the development of scaffolds with compatible mechanical properties to that of bone acting as subtracts for cell growth. Due to the poor mechanical strength, HA scaffolds could be only used as a bone substitute in low loaded bearing applications. In order to improve the mechanical behavior of HA based scaffolds, various kinds of composite scaffolds have been developed. Furthermore, the nanocomposite porous BCPS-10 wt% HA whisker scaffold with a porosity of 72% was fabricated using a combination of gel casting and polymer sponge technique. The mechanical properties of the scaffolds increased from 4 MPa (in BCPS) to 9.78 MPa (in BCPS-10% HA whisker scaffold). In this project, we showed that the addition of HT nanopowder up to 30 wt% could significantly improve the compressive strength of BCPS. It is noteworthy to mention that a uniform microstructure is an important parameter for the higher mechanical properties of the scaffolds. The in vitro bioactivity of the scaffolds

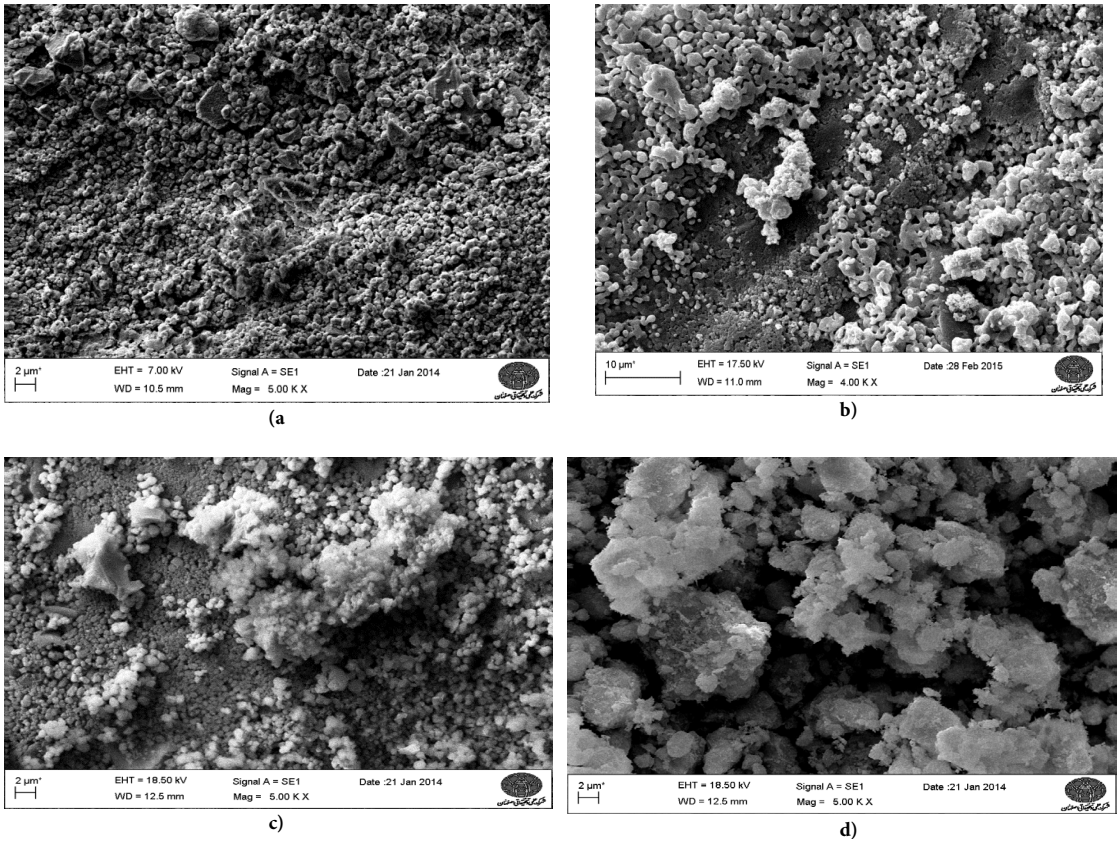


Fig. 6. Scanning electron microscopy images of a) BCP, b) BCPS-10, c) BCPS-20 and d) BCPS-30 after 28 days immersion in simulated body fluid with different resolutions

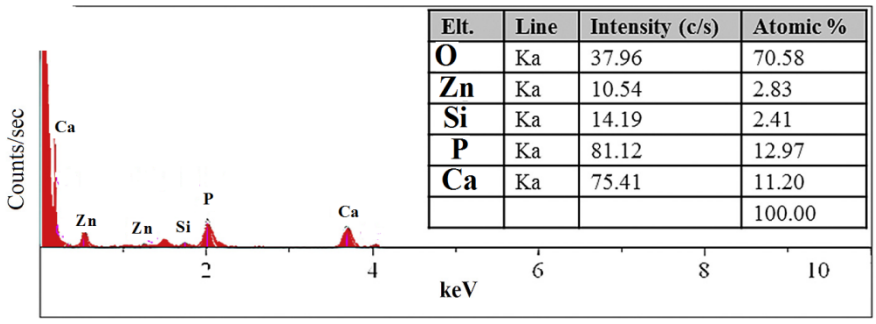


| Elt. | Line | Intensity (c/s) | Atomic % |
|---|---|---|---|
| O | Ka | 37.96 | 70.58 |
| Zn | Ka | 10.54 | 2.83 |
| Si | Ka | 14.19 | 2.41 |
| P | Ka | 81.12 | 12.97 |
| Ca | Ka | 75.41 | 11.20 |
| | | | 100.00 |

Fig. 7. Energy dispersive spectrometry spectrum of BCPS-30 after 28 days immersion in simulated body fluid.

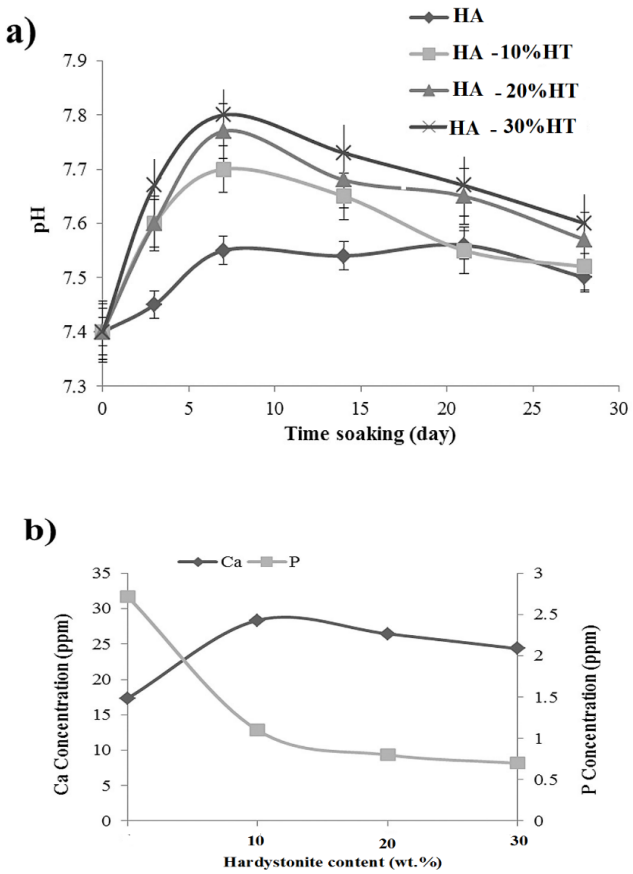


Fig. 8. a) The pH values of SBF after immersion of various scaffolds as a function of soaking time. b) The concentration profiles of calcium (Ca) and phosphorus (P) ions in the SBF at different HT contents.

was evaluated using simulated body fluid (SBF) solution. The scanning electron microscopy images of the scaffolds with different compositions, after soaking in the SBF solution for 28 days, are presented in Fig. 6. The bone like apatite with spherical particles was deposited on the surface of the scaffolds. Therefore, increasing the HT content up to 30 wt% (Fig. 6d) boosted the HA formation on the surface of the scaffolds. The deposition of apatite layer on BCPS 30 after soaking in SBF for 28 days was confirmed via energy dispersive spectrometry spectrum (Fig. 7). Compared to the EDS spectrum of the scaffolds before immersing in SBF (Fig. 5), the concentration of P and Ca ions increased confirming the formation of HA layer on the surface of the scaffolds after soaking in SBF.

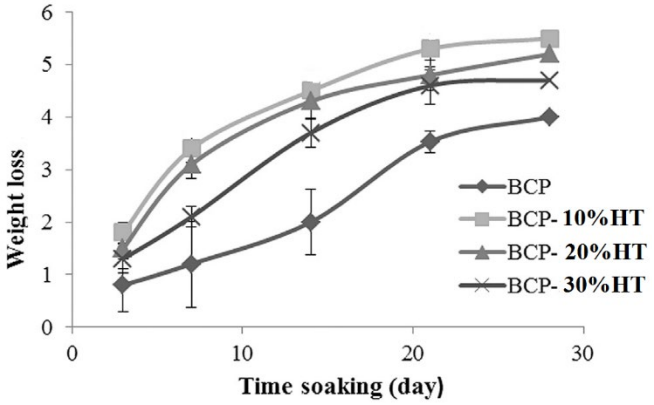


Fig. 9. The weight loss (wl.%) of different scaffolds in PBS solution as a function of soaking time.

Thus, the Zn and Si ions were detected on the surface of the scaffold due to the presence of the HT phase. Fig. 8a shows the changes of pH value of SBF during 28 days soaking of various scaffolds. The pH value of SBF was increased with increasing the HT content of the scaffolds. The pH changes graphs revealed two distinct regions; an increase in the pH up to 7 days of soaking time followed by a decrease in pH value. This behavior is in an agreement with the results obtained by other researchers who pointed out a similar trend in pH changes for other silicate based ceramics such as wolastonite), HT [18] and bioglass [30]. Fig. 9b shows Ca and P ion concentrations of simulated body fluid as a function of HT contents after 28 days of soaking. The calcium ion concentration was increased from 17.4 ppm (BCPS0) to 29.32 ppm (BCPS10) and then decreased to 25.12 ppm (BCPS30). Calcium ions released from both BCPS and HT components resulted in an enhanced Ca ion concentration in SBF. Furthermore, the concentration of phosphorus ions reduced with increasing HT contents (Fig. 9 b) as a result of the formation of the supersaturated solution around the scaffolds and deposition of Ca and P ions on the surface, which in turn implies the higher bioactivity of HT. It should be noted that rapid exchange of $Ca^{2+}$ and $Zn^{2+}$ ions with H or $H_3O$ from simulated body fluid can increase the pH and hydroxyl concentration of the solution. These changes lead to the formation of Si-OH bonds on the surface of the scaffold causing the nucleation of HA. In this part, migration of P, Ca and hydroxyl ions from the surrounding fluid to the surface of the scaffolds accelerated the nucleation of bone like HA and resulted in the reduction of pH value due to the feeding of hydroxyl ions during the formation of HA layer. The deposition of HA layer on the surface of the scaffolds could provide a suitable substrate for proliferation. Thus, a strong bond can be formed with the surrounding tissue and help the biological fixation of the scaffold in the bone defect. In this research, the precipitation of HA layer on the surface of the composite scaffolds after soaking in SBF demonstrated a higher degree of bioactivity of composite scaffolds compared to that of BCPS. So, in the previous studies, a higher bioactivity was observed for $CaO\text{-}SiO_2\text{-}ZnO$ systems such as HT compared to calcium phosphate (CP) ceramics. As seen in Fig. 10, the weight loss of the scaffolds is observed after soaking in PBS solution for up to 28 days. The weight loss (wl) of the scaffolds enhanced with increasing the soaking time and HT content, indicating the higher degradation rate of the scaffolds. It is well proved that materials with smaller grain size show a higher degradation rate in vitro. With increasing the HT content, the grain size of the scaffolds decreased in (Fig. 4b) that resulted in an increased interface between the samples and the solution, followed by a higher degradation rate of the composite scaffolds. In addition, the weight loss of the scaffolds produced in this research was lower than that of some bio-ceramics such as $CaSiO_3$ (25%) after soaking for 28 days, suggesting that these scaffolds can be used for bone defects which require a controlled slow degradation rate.

## CONCLUSION

In this research, highly porous (75%) structure less scaffolds were synthesized from hydroxyapatite and hardystonite nanopowders by the space holder technique. Moreover, adding HT nanopowder reduced the average pore and grain sizes of the

scaffolds, resulted in a three time enhancement in the compressive strength. So, the nanostructured composite scaffolds showed a higher bioactivity and biodegradability compared to the pure BCPS. Also, due to the positive role of silanol groups formed on the surface of the scaffolds, nanostructured HT/BCPS significantly promoted cell viability and proliferation compared to BCPS.

## ACKNOWLEDGMENT

The authors would like to thank the Najafabad, Islamic Azad University for their financial supports.

## CONFLICT OF INTEREST

The authors confirm that this article content has no conflict of interest.

## REFERENCES

1. Singh R, Shedbalkar UU, Wadhwani SA, Chopade BA. Bacteriagenic silver nanoparticles: synthesis, mechanism, and applications. Applied Microbiology and Biotechnology. 2015;99(11):4579-93.
2. Gheisari H, Karamian E, Abdellahi M. A novel hydroxyapatite –Hardystonite nanocomposite ceramic. Ceramics International. 2015;41(4):5967-75.
[3] Gheysari H, Karamian E. Preparation and characterization of hydroxyapatite reinforced with hardystonite as a novel bio-nanocomposite for tissue engineering. Nanomedicine Journal. 2015;2(1):141-52.
4. Karamian E, Abdellahi M, Gheisari H. Fluorine-substituted HA reinforced with zircon as a novel nano-biocomposite ceramic: Preparation and characterization. International Journal of Materials Research. 2015;106(12):1285-90.
5. Gheisari Dehsheikh H, Ghasemi-Kahrizsangi S. Performance improvement of MgO-C refractory bricks by the addition of Nano-ZrSiO 4. Materials Chemistry and Physics. 2017;202:369-76.
6. Ghasemi-Kahrizsangi S, Dehsheikh HG, Karamian E. Impact of Titania nanoparticles addition on the microstructure and properties of MgO-C refractories. Ceramics International. 2017;43(17):15472-7.
7. Ghasemi-Kahrizsangi S, Gheisari Dehsheikh H, Boroujerdnia M. Effect of micro and nano-Al 2 O 3 addition on the microstructure and properties of MgO-C refractory ceramic composite. Materials Chemistry and Physics. 2017;189:230-6.
[8] Ghasemi-Kahrizsangi S, Karamian E, Gheisari Dehsheikh H, Ghasemi-Kahrizsangi A. A Review on Recent Advances on Magnesia-Doloma Refractories by Nano-Technology. Journal of Water and Environmental Nanotechnology. 2017;2(3):206-22.
9. Iwata NY, Lee G-H, Tokuoka Y, Kawashima N. Sintering behavior and apatite formation of diopside prepared by coprecipitation process. Colloids and Surfaces B: Biointerfaces. 2004;34(4):239-45.
10. Ghasemi-Kahrizsangi S, Dehsheikh HG, Karamian E, Boroujerdnia M, Payandeh K. Effect of MgAl2O4 nanoparticles addition on the densification and properties of MgO-CaO refractories. Ceramics International. 2017;43(6):5014-9.
11. Ghasemi-Kahrizsangi S, Barati Sedeh M, Gheisari Dehsheikh H, Shahraki A, Farooghi M. Densification and properties of ZrO2 nanoparticles added magnesia–doloma refractories. Ceramics International. 2016;42(14):15658-63.
[12] Ghasemi-kahrizsangi S, Gheisari-dehsheikh H, Boroujerdnia M. The Effect of Nano Meter Size $ZrO_2$ Particles Addition on The Densification and Hydration Resistance of Magnesite– Dolomite Refractories. Iranian Journal of Materials Science & Engineering. 2016;13(4):33-40.
13. Ghasemi-Kahrizsangi S, Karamian E, Ghasemi-Kahrizsangi A, Desheikh HG, Soheily A. The impact of trivalent oxide nanoparticles on the microstructure and performance of magnesite-dolomite refractory bricks. Materials Chemistry and Physics. 2017;193:413-20.
14. Schmid G. Large clusters and colloids. Metals in the embryonic state. Chemical Reviews. 1992;92(8):1709-27.